ADP-09-09/T687

Isolating Excited States of the Nucleon in Lattice QCD

M.S. Mahbub,[1,2] Alan Ó Cais,[1] Waseem Kamleh,[1] B.G. Lasscock,[1] Derek B. Leinweber,[1] and Anthony G. Williams[1]
(CSSM Collaboration)

[1]*Special Research Centre for the Subatomic Structure of Matter, Adelaide, South Australia 5005, Australia, and Department of Physics, University of Adelaide, South Australia 5005, Australia.*
[2]*Department of Physics, Rajshahi University, Rajshahi 6205, Bangladesh.*

We discuss a robust projection method for the extraction of excited-state masses of the nucleon from a matrix of correlation functions. To illustrate the algorithm in practice, we present results for the positive parity excited states of the nucleon in quenched QCD. Using eigenvectors obtained via the variational method, we construct an eigenstate-projected correlation function amenable to standard analysis techniques. The method displays its utility when comparing results from the fit of the projected correlation function with those obtained from the eigenvalues of the variational method. Standard nucleon interpolators are considered, with 2×2 and 3×3 correlation matrix analyses presented using various combinations of source-smeared, sink-smeared and smeared-smeared correlation functions. Using these new robust methods, we observe a systematic dependency of the extracted nucleon excited-state masses on source- and sink-smearing levels. To the best of our knowledge, this is the first clear indication that a correlation matrix of standard nucleon interpolators is insufficient to isolate the eigenstates of QCD.

PACS numbers: 11.15.Ha,12.38.Gc,12.38.-t

I. INTRODUCTION

Lattice QCD provides a non-perturbative tool to explore many properties of hadrons from first principles. In the case of the hadron mass spectrum there are well developed methods to compute the mass spectra. However, while the extraction of the ground states of the hadron spectrum is a well understood problem, and has provided impressive agreement with experimental results [1], the excited states still prove a significant challenge. The Euclidean-time correlation function provides access to a tower of states since it is a sum of decaying exponentials with the masses of the states in the exponents. The ground state mass, being the lowest energy state and thereby having the slowest decay rate, is obtained by analysis of the large time behaviour of this function. The excited states, however, belong to the sub-leading exponentials of the two-point correlation function. Extracting excited states masses from these sub-leading exponents is difficult as the correlation functions decay quickly and the signal to noise ratio deteriorates more rapidly.

One of the long-standing puzzles in hadron spectroscopy has been the low mass of the first positive parity, $J^P = \frac{1}{2}^+$, excitation of the nucleon, known as the Roper resonance $N^*(1440$ MeV). In constituent or valence quark models with harmonic oscillator potentials, the lowest-lying odd parity states naturally occurs below the $N = \frac{1}{2}^+$ state (with principal quantum number $N = 2$) [2, 3] whereas, in nature the Roper resonance is almost 100 MeV below the $N = \frac{1}{2}^-(1535$ MeV) state. Similar difficulties in the level orderings appear for the $J^P = \frac{3}{2}^+\Delta^*(1600)$ and $\frac{1}{2}^+\Sigma^*(1690)$ resonances, which have led to the speculation that the Roper resonance may be more appropriately viewed as a hybrid baryon state with explicitly excited glue field configurations [4, 5] or as a breathing mode of the ground state [6] or states which can be described in terms of meson-baryon dynamics alone [7]. The first detailed analysis of the positive parity excitation of nucleon was performed in Ref. [8] using Wilson fermions and an operator product expansion spectral ansatz. Since then several attempts have been made to address these issues in the lattice framework [9, 10, 11, 12, 13, 14, 15, 16], but in many cases no potential identification of the Roper state has been made [9, 10, 11, 12, 13]. Recently however, in the analysis of [14, 15, 17], a low-lying Roper state has been observed by using advanced fitting techniques [18, 19] based on Bayesian priors. Significant finite volume effects on the first positive parity $\mathrm{N}^{\frac{1}{2}^+}$ state have been observed in Refs. [16, 20, 21] using the Maximum Entropy Method [18, 19, 22, 23, 24]. Here, we use another state-of-the-art approach, namely 'the variational method' [25, 26, 27], which is based on the correlation matrix analysis and has been used quite extensively in Refs. [1, 11, 12, 27, 28, 29, 30, 31, 32, 33, 34, 35, 36, 37, 38, 39, 40, 41, 42, 43] with the first analysis of the nucleon performed by Sasaki *et al* [11]. Though the ground state mass of the nucleon has been described successfully, an unambiguous determination of the Roper state has not been successful to date with this method, though significant amounts of research have been carried out in Ref. [11, 28], the CSSM Lattice Collaboration [12, 29, 31], the BGR [1, 32, 33, 34, 35] collaboration and in Refs. [41, 42].

In this paper, we discuss an analysis method to extract masses of the nucleon from the correlation functions using a variational analysis. Employing standard interpolating operators χ_1, χ_2 and χ_4, we discuss the method for 2×2 and 3×3 correlation matrices with the point and a range of sweeps of Gaussian smearing [44] at the source, sink and at both source and sink. This analysis shows for the first time (and despite the fact that people have been

using source smeared correlation functions for quite long time [1, 12, 13, 30, 31, 32, 33, 36, 38, 45, 46, 47, 48, 49]) that, unexpectedly, the excited states of the nucleon are smearing dependent. This analysis indicates that significant caution should be taken when employing a particular level of smearing. To ensure the maximal independence of our results on human input and minimal errors, we construct a 'robot' algorithm, governed by defined fitting criteria, that automatically performs a standardised fitting procedure. We present here results from this algorithm and also those obtained from the eigenvalues to provide confidence in the extraction of the nucleon mass spectrum.

This paper is arranged as follows: Section II contains the general description of the extraction of masses with the introduction of different nucleon interpolating fields. The lattice details are in Section III, the analysis method is presented in Section IV, and conclusions are presented in Section V.

II. MASS OF HADRONS

The masses of hadrons are extracted from two-point correlation functions using operators chosen to have overlap with desired states. Let us consider a baryon state B of spin half, if we suppress Dirac indices a two point function can be written as,

$$G_{ij}(t,\vec{p}) = \sum_{\vec{x}} e^{-i\vec{p}.\vec{x}} \langle \Omega | T\{\chi_i(x)\bar{\chi}_j(0)\} | \Omega \rangle. \quad (1)$$

The operator $\chi_j(0)$ creates states from the vacuum at space-time point 0 and, following the evolution of the states in time t, the states are destroyed by the operator $\chi_i(x)$ at point x. T stands for the time ordered product of operators. Having a complete set of momentum eigenstates requires that,

$$\sum_{B,\vec{p'},s} |B,\vec{p'},s\rangle\langle B,\vec{p'},s| = I, \quad (2)$$

where B can include multi-particle states. The substitution of Eq.(2) into the Eq.(1) yields,

$$G_{ij}(t,\vec{p}) = \sum_{\vec{x}} \sum_{B,\vec{p'},s} e^{-i\vec{p}.\vec{x}} \langle \Omega|\chi_i(x)|B,\vec{p'},s\rangle\langle B,\vec{p'},s|\bar{\chi}_j(0)|\Omega\rangle. \quad (3)$$

We can express the operator $\chi_i(x)$ as

$$\chi_i(x) = e^{iP.x}\chi_i(0)e^{-iP.x}, \quad (4)$$

where, $P^\mu = P = (H,\vec{P})$ and $\vec{P}$ is the momentum operator whose eigenvalue is the total momentum of the system. Eq.(3) can now be written as,

$$\begin{aligned} G_{ij}(t,\vec{p}) &= \sum_{\vec{x}} \sum_{B,\vec{p'},s} e^{-i\vec{p}.\vec{x}} \langle \Omega|e^{iPx}\chi_i(0)e^{-iPx}|B,\vec{p'},s\rangle\langle B,\vec{p'},s|\bar{\chi}_j(0)|\Omega\rangle \\ &= \sum_{\vec{x}} \sum_{B,\vec{p'},s} e^{-iE_Bt}e^{-i\vec{x}.(\vec{p}-\vec{p'})} \langle \Omega|\chi_i(0)|B,\vec{p'},s\rangle\langle B,\vec{p'},s|\bar{\chi}_j(0)|\Omega\rangle. \end{aligned} \quad (5)$$

As we move from Minkowski space to Euclidean space, the time $t \to -it$ and the above equation then can be written as,

$$\begin{aligned} G_{ij}(t,\vec{p}) &= \sum_{B,\vec{p'},s} e^{-E_Bt}\delta_{\vec{p},\vec{p'}} \langle \Omega|\chi_i(0)|B,\vec{p'},s\rangle\langle B,\vec{p'},s|\bar{\chi}_j(0)|\Omega\rangle \\ &= \sum_{B}\sum_{s} e^{-E_Bt} \langle \Omega|\chi_i(0)|B,\vec{p},s\rangle\langle B,\vec{p},s|\bar{\chi}_j(0)|\Omega\rangle. \end{aligned} \quad (6)$$

The overlap of the interpolating fields $\chi(0)$ and $\bar{\chi}(0)$ with positive and negative parity baryon states $|B^\pm\rangle$ can be parametrized by a complex quantity called the coupling strength, $\lambda_{B^\pm}$, which can be defined for positive parity states by

$$\langle \Omega|\chi(0)|B^+,\vec{p},s\rangle = \lambda_{B^+}\sqrt{\frac{M_{B^+}}{E_{B^+}}}u_{B^+}(\vec{p},s), \quad (7)$$

$$\langle B^+,\vec{p},s|\bar{\chi}(0)|\Omega\rangle = \bar{\lambda}_{B^+}\sqrt{\frac{M_{B^+}}{E_{B^+}}}\bar{u}_{B^+}(\vec{p},s). \quad (8)$$

For the negative parity states the definition is

$$\langle \Omega|\chi(0)|B^-,\vec{p},s\rangle = \lambda_{B^-}\sqrt{\frac{M_{B^-}}{E_{B^-}}}\gamma_5 u_{B^-}(\vec{p},s), \quad (9)$$

$$\langle B^-,\vec{p},s|\bar{\chi}(0)|\Omega\rangle = -\bar{\lambda}_{B^-}\sqrt{\frac{M_{B^-}}{E_{B^-}}}\bar{u}_{B^-}(\vec{p},s)\gamma_5. \quad (10)$$

Here, $\lambda_{B^\pm}$ and $\bar{\lambda}_{B^\pm}$ are the couplings of the interpolating functions at the sink and the source respectively and $M_{B^\pm}$ is the mass of the state $B^\pm$. $E_{B^\pm}$ is the energy of the state $B^\pm$, where $E_{B^\pm} = \sqrt{M^2_{B^\pm} + \vec{p}^2}$, and $u_{B^\pm}(\vec{p},s)$ and $\bar{u}_{B^\pm}(\vec{p},s)$ are the Dirac spinors,

$$\bar{u}^\alpha_{B^\pm}(\vec{p},s)u^\beta_{B^\pm}(\vec{p},s) = \delta^{\alpha\beta}. \quad (11)$$

Thus, Eq.(6) contains a projection operator $\Gamma_\pm = \sum_s u^\beta_{B^\pm}(\vec{p},s)\bar{u}^\alpha_{B^\pm}(\vec{p},s)$, through which the contributions to the even and odd parity states from the correlation function can be obtained. For positive parity, this can be expressed as,

$$\sum_s u^\beta_{B^+}(\vec{p},s)\bar{u}^\alpha_{B^+}(\vec{p},s) = \frac{\gamma.p + M_{B^+}}{2E_{B^+}}, \quad (12)$$

and for the negative parity,

$$\gamma_5\left(\sum_s u^\beta_{B^-}(\vec{p},s)\bar{u}^\alpha_{B^-}(\vec{p},s)\right)\gamma_5 = \frac{-\gamma.p + M_{B^-}}{2E_{B^-}}. \quad (13)$$

By substituting the above Eqs. for the positive and negative parity states in Eq.(6) we obtain,

$$\mathcal{G}_{ij}(t,\vec{p}) = \sum_{B^+}\lambda_{B^+}\bar{\lambda}_{B^+}e^{-E_{B^+}t}\frac{\gamma.p_{B^+} + M_{B^+}}{2E_{B^+}} + \sum_{B^-}\lambda_{B^-}\bar{\lambda}_{B^-}e^{-E_{B^-}t}\frac{-\gamma.p_{B^-} + M_{B^-}}{2E_{B^-}}. \quad (14)$$

At momentum $\vec{p} = \vec{0}$, $E_{B^\pm} = M_{B^\pm}$, and a parity projection operator $\Gamma_\pm$ can be introduced,

$$\Gamma_\pm = \frac{1}{2}(1 \pm \gamma_0). \quad (15)$$

We can isolate the masses of the even and odd parity states by taking the trace of $\mathcal{G}$ with the operators Γ_+ and Γ_-. The positive parity state propagates through the (1,1) and (2,2) elements of the Dirac matrix, whereas, negative parity state propagates through the (3,3) and (4,4) elements.

The correlation function for positive and negative parity states can then be written as,

$$G^\pm_{ij}(t,\vec{0}) = \mathrm{Tr}_{\mathrm{sp}}[\Gamma_\pm\mathcal{G}_{ij}(t,\vec{0})] = \sum_{B^\pm}\lambda^\pm_i\bar{\lambda}^\pm_j e^{-M_{B^\pm}t}. \quad (16)$$

The correlation function contains a superposition of states. The mass of the lowest state, $M_{0^\pm}$ can be extracted at large t where the contributions from all other states are suppressed,

$$G^\pm_{ij}(t,\vec{0}) \overset{t\to\infty}{=} \lambda^\pm_{i0}\bar{\lambda}^\pm_{j0}e^{-M_{0^\pm}t}. \quad (17)$$

The source smearing [44] technique is applied to increase the overlap of the interpolators with the lower lying states. A fixed boundary condition in the time direction is applied for the fermions by setting $U_t(\vec{x},N_t) = 0\,\forall\,\vec{x}$ in the hopping terms of the fermion action with periodic boundary conditions imposed in the spatial directions. Gauge invariant Gaussian smearing [44] in the spatial dimensions is applied through an iterative process. The smearing procedure is:

$$\psi_i(x,t) = \sum_{x'}F(x,x')\psi_{i-1}(x',t), \quad (18)$$

where,

$$F(x,x') = (1-\alpha)\delta_{x,x'} + \frac{\alpha}{6}\sum_{\mu=1}^{3}[U_\mu(x)\delta_{x',x+\hat{\mu}} + U^\dagger_\mu(x-\hat{\mu})\delta_{x',x-\hat{\mu}}], \quad (19)$$

where the parameter $\alpha = 0.7$ is used in our calculation. After repeating the procedures N_{sm} times on a point source the resulting smeared fermion field is,

$$\psi_{N_{\mathrm{sm}}}(x,t) = \sum_{x'}F^{N_{sm}}(x,x')\psi_0(x',t). \quad (20)$$

The extraction of the ground state mass is done straightforwardly. However access to the excited state masses requires additional effort. Here we consider the variational method [25, 26, 27]. The variational method requires the cross correlation of operators so that the operator space can be diagonalised and the excited state masses extracted from the exponential nature of the diagonalised basis. To access N states of the spectrum, one requires a minimum of N interpolators. Traditionally, only a few interpolators are considered providing access to a small number of states of the desired channel.

The parity projected two point correlation function matrix for $\vec{p} = 0$ can be written as,

$$G_{ij}(t) = (\sum_{\vec{x}}\mathrm{Tr}_{\mathrm{sp}}\{\Gamma_\pm\langle\Omega|\chi_i(x)\bar{\chi}_j(0)|\Omega\rangle\}) \quad (21)$$

$$= \sum_{\alpha=0}^{N-1}\lambda^\alpha_i\bar{\lambda}^\alpha_j e^{-m_\alpha t}. \quad (22)$$

Here, λ^α_i and $\bar{\lambda}^\alpha_j$ are the couplings of interpolators χ_i and $\bar{\chi}_j$ at the sink and source respectively to eigenstates $\alpha = 0,\cdots,(N-1)$. m_α is the mass of the state α. The N interpolators have the same quantum numbers and provide an N-dimensional basis upon which to describe the states. Using this basis we aim to construct N independent interpolating source and sink fields which isolate N baryon states $|B_\alpha\rangle$, *i.e.*

$$\bar{\phi}^\alpha = \sum_{i=1}^{N}u^\alpha_i\bar{\chi}_i, \quad (23)$$

$$\phi^\alpha = \sum_{i=1}^{N} v_i^\alpha \chi_i, \tag{24}$$

such that,

$$\langle B_\beta, p, s|\bar{\phi}^\alpha|\Omega\rangle = \delta_{\alpha\beta}\bar{z}^\alpha \bar{u}(\alpha, p, s), \tag{25}$$

$$\langle \Omega|\phi^\alpha|B_\beta, p, s\rangle = \delta_{\alpha\beta} z^\alpha u(\alpha, p, s), \tag{26}$$

where z^α and $\bar{z}^\alpha$ are the coupling strengths of ϕ^α and $\bar{\phi}^\alpha$ to the state $|B_\alpha\rangle$. Consider a real eigenvector u_j^α which operates on the correlation matrix $G_{ij}(t)$ from right, one can obtain [12],

$$\begin{aligned} G_{ij}(t)u_j^\alpha &= (\sum_{\vec{x}} \mathrm{Tr}_{\mathrm{sp}}\{\Gamma_\pm \langle\Omega|\chi_i\bar{\chi}_j|\Omega\rangle\})u_j^\alpha \\ &= \lambda_i^\alpha \bar{z}^\alpha e^{-m_\alpha t}. \end{aligned} \tag{27}$$

For notational convenience, in the remainder of the discussion the repeated indices i, j, k are to be understood as being summed over, whereas, α, which stands for a particular state, is not. Since the only t dependence comes from the exponential term, we can write a recurrence relation at time $(t + \triangle t)$ as,

$$G_{ij}(t + \triangle t)u_j^\alpha = e^{-m_\alpha \triangle t} G_{ij}(t)u_j^\alpha. \tag{28}$$

If we multiply the above equation by $[G_{ij}(t)]^{-1}$ from the left we get,

$$\begin{aligned} [(G(t))^{-1}G(t + \triangle t)]u^\alpha &= e^{-m_\alpha \triangle t}u^\alpha \\ &= c^\alpha u^\alpha. \end{aligned} \tag{29}$$

This is an eigenvalue equation for eigenvector u^α with eigenvalue $c^\alpha = e^{-m_\alpha \triangle t}$. We can also solve the left eigenvalue equation to recover the v^α eigenvector,

$$v_i^\alpha G_{ij}(t + \triangle t) = e^{-m_\alpha \triangle t} v_i^\alpha G_{ij}(t). \tag{30}$$

Similarly,

$$v^\alpha [G(t + \triangle t)(G(t))^{-1}] = e^{-m_\alpha \triangle t} v^\alpha. \tag{31}$$

The vectors u_j^α and v_i^α diagonalize the correlation matrix at time t and $t + \triangle t$ making the projected correlation matrix,

$$v_i^\alpha G_{ij}(t)u_j^\beta = \delta^{\alpha\beta} z^\alpha \bar{z}^\beta e^{-m_\alpha t}. \tag{32}$$

The parity projected, eigenstate projected correlator, $v_i^\alpha G_{ij}^\pm(t)u_j^\alpha \equiv G_\pm^\alpha$ is then used to obtain masses of different states. We construct the effective mass

$$\begin{aligned} M_{\mathrm{eff}}^\alpha(t) &= \ln\left(\frac{G_\pm^\alpha(t, \vec{0})}{G_\pm^\alpha(t + 1, \vec{0})}\right) \\ &= M_\pm^\alpha. \end{aligned} \tag{33}$$

and apply standard analysis techniques as described in the following.

III. LATTICE DETAILS

We use an ensemble of 200 quenched configurations with a lattice volume of $16^3 \times 32$. Gauge field configurations are generated by using the DBW2 gauge action [50, 51] and an $\mathcal{O}(a)$-improved FLIC fermion action [52] is used to generate quark propagators. This action has excellent scaling properties and provides near continuum results at finite lattice spacing [53]. The lattice spacing is $a = 0.1273$ fm, as determined by the static quark potential, with the scale set with the Sommer scale, $r_o = 0.49$ fm [54]. In the irrelevant operators of the fermion action we apply four sweeps of stout-link smearing to the gauge links to reduce the coupling with the high frequency modes of the theory [55]. We use the same method as in Ref. [45] to determine fixed boundary effects, and the effects are significant only after time slice 25 in the present analysis. Beside point operators, various sweeps (1, 3, 7, 12, 16, 26, 35, 48, 65 sweeps corresponding to rms radii, in lattice units, 0.6897, 1.0459, 1.5831, 2.0639, 2.3792, 3.0284, 3.5237, 4.1868, 5.0067) of gauge invariant Gaussian smearing [44] are applied at the source (at $t = 4$) and at the sink. This is to ensure a variety of overlaps of the interpolators with the lower-lying states. The analysis is performed on four different quark masses providing pion masses $m_\pi = \{0.797, 0.729, 0.641, 0.541\}$ GeV. The error analysis is performed using a second-order single elimination jackknife method, where the χ^2/dof is obtained via a covariance matrix analysis method. We discuss our fitting method in the next section.

The nucleon interpolators we consider in this analysis are,

$$\chi_1(x) = \epsilon^{abc}(u^{Ta}(x)C\gamma_5 d^b(x))u^c(x) \tag{34}$$

$$\chi_2(x) = \epsilon^{abc}(u^{Ta}(x)C d^b(x))\gamma_5 u^c(x) \tag{35}$$

$$\chi_4(x) = \epsilon^{abc}(u^{Ta}(x)C\gamma_5\gamma_4 d^b(x))u^c(x) \tag{36}$$

The χ_1 and χ_2 interpolators are used in Refs. [8, 11, 56]. The χ_4 interpolator is considered as the time component of the χ_3 interpolator used in Refs.[29, 31, 32]. We use the Dirac representation of the gamma matrices in our analysis.

IV. ANALYSIS AND DISCUSSION

A. Correlation Matrix Analysis

We begin this section by outlining the fitting method used in this paper. The method is based on the maximisation of the Euclidean-time fit window and the minimisation of the value of the χ^2/dof commencing at the earliest time possible [57]. At larger times the lighter states dominate the correlation function. However, the signal to noise ratio decreases rapidly, forcing increased errors in the results. Additionally, ignoring smaller time slices may lead to eliminating important information about ex-

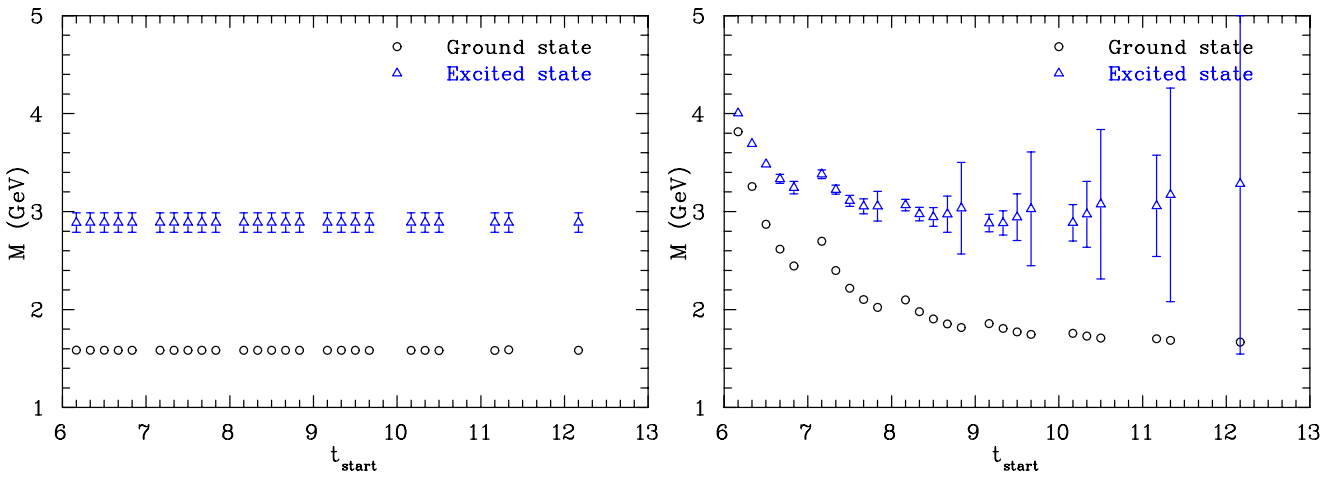

FIG. 1: (Color online). Mass of the nucleon ($N^{\frac{1}{2}^+}$) from the projected correlation function as shown in Eq.32 (left) and from the eigenvalue (right) for a 2×2 correlation matrix of χ_1, χ_2 interpolators. The figure corresponds to a pion mass of 797 MeV (heaviest) and for the **point source** to **point sink** correlation functions. Each pair of ground and excited states masses correspond to the diagonalization of the correlation matrix for each set of variational parameters $t_{\rm start}$ (shown in major tick marks) and $\triangle t$ (shown in minor tick marks). Here, the time t as shown in Eqs.(29, and 31) is called $t_{\rm start}$.

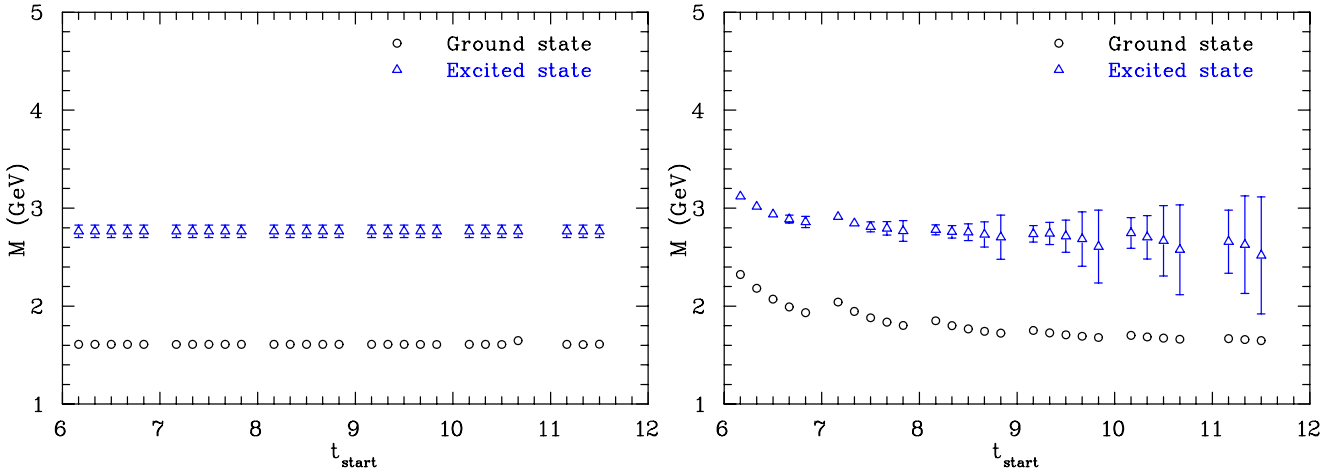

FIG. 2: (Color online). As in Fig. 1, but for **source smeared** to **point sink** correlation functions with the number of Gaussian smearing sweeps set to 7, which corresponds to a smearing radius of 1.5831 in lattice units.

cited states included in the two-point correlation function [58]. Data at larger time slices for excited states extracted using the variational method can be contaminated by residual contributions from the lower lying states, resulting in lower values of excited states mass. In consideration of these points, in this analysis we use a preference towards earlier times which have a high signal to noise ratio and are therefore heavily constraining in the fit procedure. This allows us to isolate the energy level from higher state contamination through the χ^2/dof and simultaneously control the errors potentially introduced at higher times (where the signal to noise ratio is lower) by contamination from lower-lying states in the varitiational analysis procedure. Hence, the inclusion of these early times minimizes the error in the results while an acceptable value of χ^2/dof is maintained.

We perform the analysis for 2×2 and 3×3 correlation matrices via the variational method. For the quark masses considered herein, the interpolator χ_1 has better overlap with the lower-energy states [12] and strongly couples to the nucleon ground state [11, 32], whereas the interpolator χ_2 does not have good overlap with the nucleon ground state and couples to the higher energy state(s) [8, 11, 12, 59]. We have found that the other interpolator, χ_4, is very similar to χ_1 and also couples strongly to the ground state [32], which suggests that the χ_1 and χ_4 operators are somewhat linearly dependent to each other. We call the start time, t, of the variational analysis $t_{\rm start}$.

The diagonalization is accomplished for different values of $t_{\rm start}$ with a few values of $\triangle t$, here $\triangle t = 1 - 5$ for each $t_{\rm start}$.

We now consider fits to the parity and eigenstate projected effective mass of Eq.(33) which follows from the eigenvector analysis. In this presentation, we consider the cut-off value for an acceptable value of χ^2/dof as 1.30. Firstly, we try to fit the effective mass from two time slices after the source to the largest possible time of the correlation function i.e., from time slice 6 (since the source is at 4) to time slice 25 (after which the fixed boundary effects are significant). We call the lower time $t_{\rm min}$ and the larger time $t_{\rm max}$. If an acceptable fit is not obtained then we keep $t_{\rm min}$ fixed and decrease $t_{\rm max}$ and reattempt a fit. If this is also unsuccessful then we iterate the same process until we reach a time near $t_{\rm min}$ while maintaining a minimum fit window size. At this point, if an acceptable fit (as dictated by the χ^2/dof) is still not obtained then we increase $t_{\rm min}$ by one time slice and try to fit the new window $t_{\rm min}$ to $t_{\rm max}$. This process repeats until a fit is obtained. The minimum fit window size we consider for the ground state is 5 time slices in the effective mass which corresponds to 6 time slices in $G(t)$. For the excited states, the minimum window size of 3 is considered corresponding to 4 time slices in $G(t)$. This provides a balance in providing evidence of an eigenstate while avoiding residual contaminations of lower-lying states.

Figs. 1 and 2 present the ground and excited states of the nucleon for a 2×2 correlation matrix with χ_1 and χ_2 interpolators for point and smeared source correlation functions respectively. The point-like correlation function is a difficult correlator to extract a mass from, as it admits strong overlap with excited states. Nevertheless, we consider the point correlation function as a challenge in this analysis.

The left and right figures show the mass from the projected correlation function and the mass from the eigenvalue respectively. Each point corresponds to the diagonalization of the matrix for each set of variational parameters $t_{\rm start}$ and $\triangle t$. The mass coming from eigenvalues are intrinsic to the variational analysis since they come directly from the diagonalization of the matrix, while the mass from the projected correlation function comes from the 'robot' algorithm described above. It is interesting to note that masses from the projected correlation functions are almost independent of the variational parameters. Fig. 1 also shows that mass can also be extracted reliably from the point-to-point correlation function. The behaviour of the eigenvalues at lower $t_{\rm start}$ and $\triangle t$ reflects the contamination of higher excited states. Although it can be difficult to extract a mass directly from the eigenvalues, it is relatively easy to expose a mass in the projected correlation function.

Figs. 3 and 4 show the eigenvectors for the diagonalisation of correlation matrices for the point (for Fig. 1) and source-smeared (for Fig. 2), correlation functions respectively. Eigenvectors are normalized for each set of variational parameters to unit length. It is interesting to note that the eigenvectors do not show a strong sensitivity to excited-state contamination. As with the mass from the eigenvalue, at larger $t_{\rm start}$, the eigenvectors are also dominated by errors. Eigenvectors in Figs. 3 and 4 also indicate that as the χ_1 and χ_2 interpolators are much orthogonal to each other [12], the χ_1 interpolator has little influence over the excited state and the χ_2 interpolator also contributes very little to the nucleon ground state.

Figs. 5 and 6 show the ground and excited state mass of the nucleon (as in Figs. 1 and 2) for χ_1 and χ_4 interpolators. The excited state mass for the point correlation function, Fig. 5, starts a little from below and settles down after a few values of $t_{\rm start}$. It should be noted that similar effects also persist in the 3×3 correlation matrix analysis where both χ_1 and χ_4 operators are present. However, this behaviour diminishes with the level of smearing as shown in Fig. 6.

The correlation matrix analysis of χ_1 and χ_4 interpolators provide nontrivial mixing as illustrated in Figs. 7 and 8. As discussed earlier, χ_1 and χ_4 are very similar and there is little to separate them. This is illustrated in Fig. 7 which shows some drift in the eigenvectors for the ground state, but with little variance in the ground-state mass.

Fig. 9 presents eigenvectors of the 3×3 correlation matrix of χ_1, χ_2 and χ_4 interpolators for the point-to-point correlation functions. As χ_1 and χ_4 interpolators largely couple to the ground state, the left figure in Fig. 9 shows the higher contributions to the ground state come from the χ_1 and χ_4 interpolators, while the first excited state (middle figure) is completely dominated by χ_2 interpolator and in the second excited state (right figure) contributions from all the interpolators are distributed.

To select a single mass from a series of $t_{\rm start}$ and $\triangle t$, a value of $t_{\rm start} = 8$ is preferred, and $\triangle t \geq 4$ (if possible). We prefer to avoid the value of $\triangle t = 1$, as it appears that $\triangle t = 1$ is, in a few cases, more prone to fluctuations than larger values. If a mass is not obtained for these parameters (this is the case for the lighter quark masses), then we decrease $\triangle t$ by one time slice and try to obtain a diagonalisation. This procedure is repeated until the value $t_{\rm start} + \triangle t = 10$ is reached. If the diagonalisation is still not obtained then we decrease $t_{\rm start}$ and repeat the same procedure. We note that our experience is in accord with that of Ref. [60, 61]. In practice we emphasise the importance of keeping $t_{\rm start} + \triangle t$ large [61].

B. Smearing Dependency of Excited States

Now we discuss the smearing dependency we have observed in the masses of the excited states. In Figs. 1 and 2, a careful comparison of the masses for point- and source-smeared correlation functions reveals that the excited state mass for the source-smeared case is lower in value than for the point source. In contrast, the ground

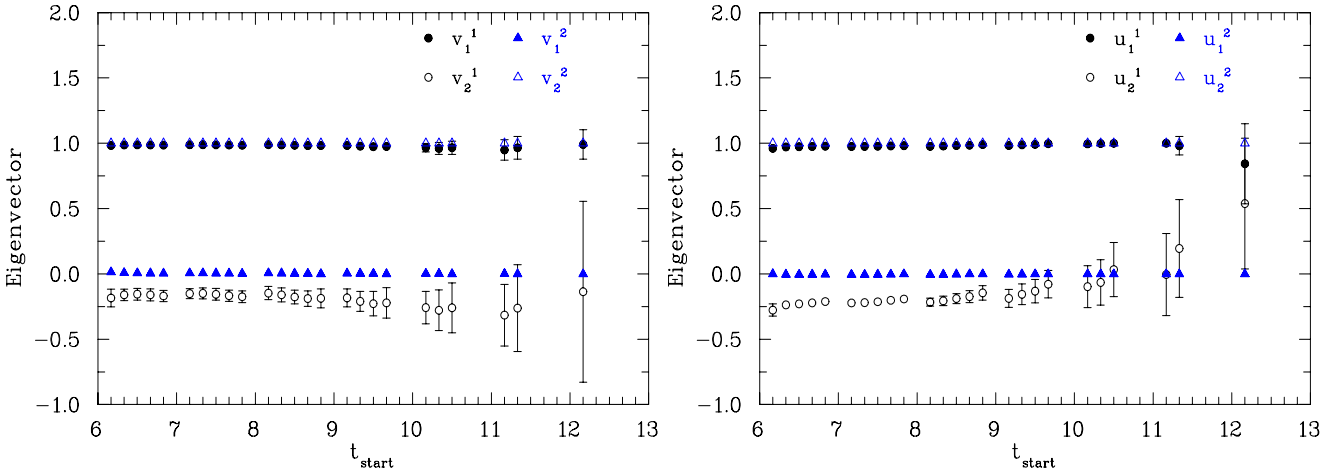

FIG. 3: (Color online). Eigenvector values for v_i^α (left) and u_i^α (right), as shown in Eq.(32), for the correlation matrix analysis of Fig. 1. The superscript α stands for the eigenstates while the subscript i represents the interpolators. Here, for the 2x2 correlation matrix, $\alpha = 1, 2$ and $i = 1, 2$.

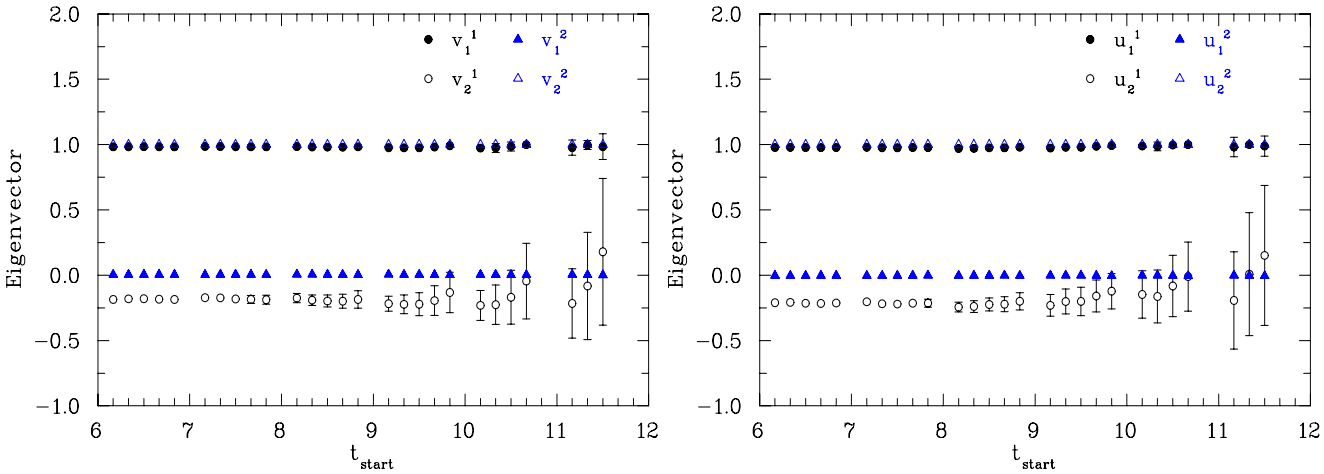

FIG. 4: (Color online). As in Fig. 3, but for the correlation matrix analysis of Fig. 2.

state masses agree within one standard deviation for almost all sets of variational parameters.

Here we extend the analysis for various amounts of source-smearing sweeps in the correlation functions. Our new robust analysis techniques reveal that the excited-state mass is smearing dependent. In Figs. 10 and 11, the ground-state mass reveals no significant dependence on smearing. However, the masses of the excited state show a distinct systematic dependence on the smearing radius. Horizontal lines are drawn at the radius ~ 3.52 (no. of sweeps = 35) to aid in illustrating the absence of source invariance. Fig. 11 presents similar results for the lightest quark mass considered in this analysis.

One might search for an optimal level of smearing where the excited state mass plateaus indicating overlap with a neighbouring state is minimized. However, there is no evidence of a plateau in Figs. 10 and 11.

This behaviour is also present for our 3×3 correlation matrix analysis as illustrated in Fig. 12. Here it is found that the two excited states are almost degenerate and display a similar dependence on the source smearing parameters.

Thus, we must conclude that the standard analysis of the 3×3 correlation matrix of χ_1, χ_2 and χ_4 interpolators is insufficient to isolate the energy eigenstates. The first excited-state mass revealed here is due to a linear combination of mass eigenstates and therefore is likely to sit high relative to the first excited eigenstate mass.

In Fig. 13, we present results for a variational analysis of smeared-smeared correlation functions. The result from the 3×3 correlation matrix analysis is shown in Fig. 14. In this case we also observe two nearly-degenerate excited states. While there is some suggestion of a plateau in this case, it seems unlikely to us that

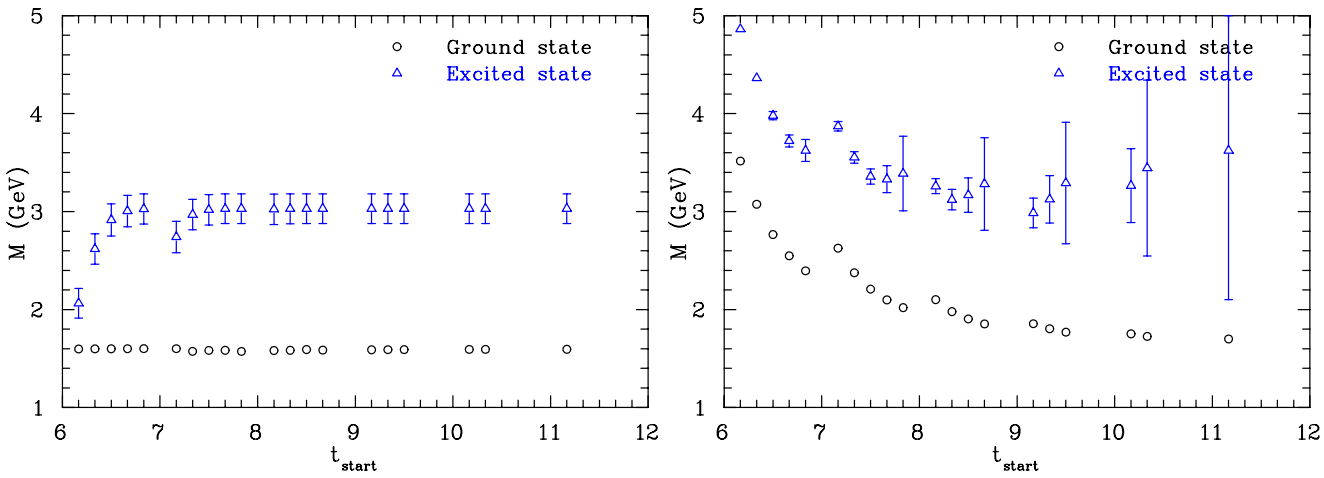

FIG. 5: (Color online). Mass of the nucleon ($N^{\frac{1}{2}^+}$) from the projected correlation function as shown in Eq.32 (left) and from the eigenvalue (right) for a 2×2 correlation matrix of χ_1 and χ_4 interpolators. The figure corresponds to a pion mass of 797 MeV and for the **point source** to **point sink** correlation functions. Each pair of ground and excited states masses correspond to the diagonalization of the correlation matrix for each set of variational parameters $t_{\rm start}$ (shown in major tick marks) and $\triangle t$ (shown in minor tick marks).

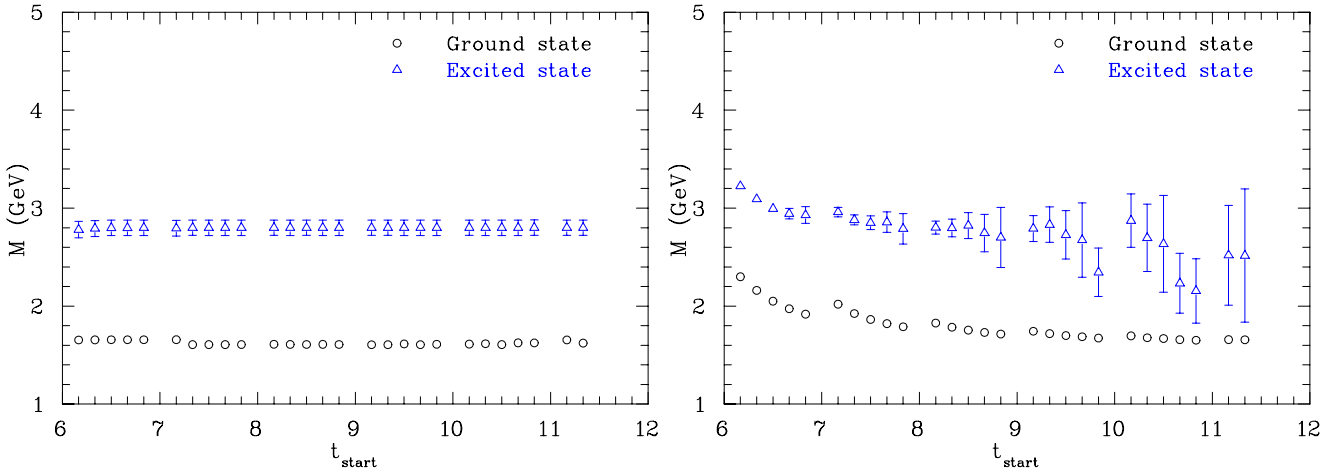

FIG. 6: (Color online). As in Fig. 5, but for the **source smeared** to **point sink** correlation functions with the number of Gaussian smearing sweeps at 7, which corresponds to a smearing radius of 1.5831 in lattice unit.

the masses revealed here are true eigenstate masses.

It is important to consider the impact of the finite volume of the lattice on our observations. It is well known that the eigenstate energies have a volume dependence and will change as one changes the volume [16, 20, 21]. However, as we consider only one fixed volume, the eigenstate energies are fixed. Thus the variation of the excited state mass revealed as our interpolating fields change can only be due to a superposition of eigenstates in the effective mass function.

V. CONCLUSION

In this study we have defined and demonstrated a robust technique for the analysis of correlation function matrices. We have observed that the eigenvectors describing the optimal overlap of interpolating fields for isolating the first excited state are insensitive to the parameters of the eigenvector analysis. This approximate invariance of the eigenvectors is in sharp contrast to the eigenvalue itself. The latter changes significantly as the starting time and the change in time is varied. To create a robust technique for the extraction of the excited state mass, we exploit the invariance of the eigenvectors and construct an eigen-projected correlation function. This

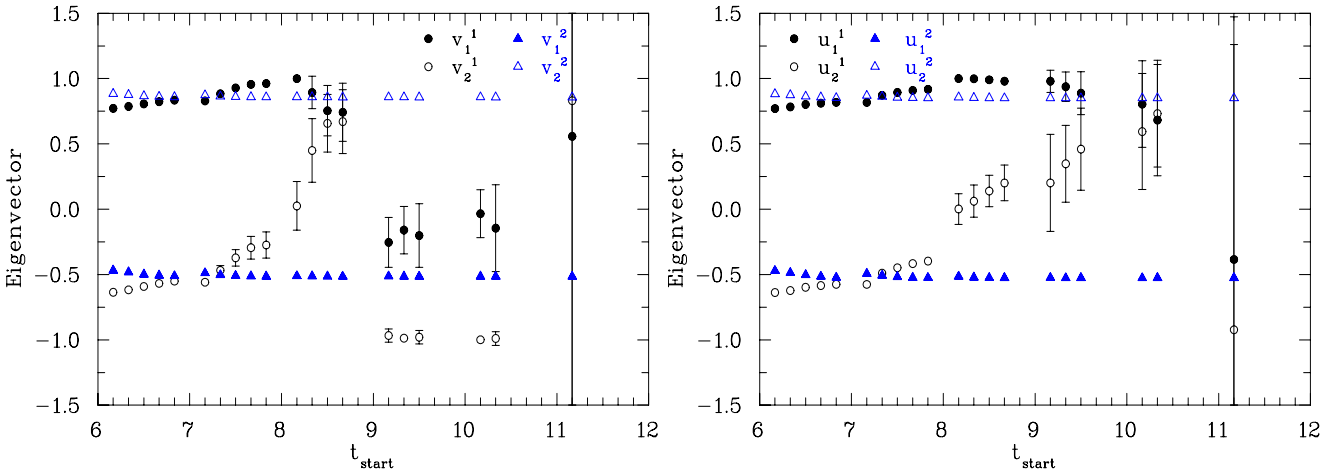

FIG. 7: (Color online). Eigenvector values of v_i^α (left) and u_i^α (right), as shown in Eq.(32), for the correlation matrix analysis of Fig.(5).

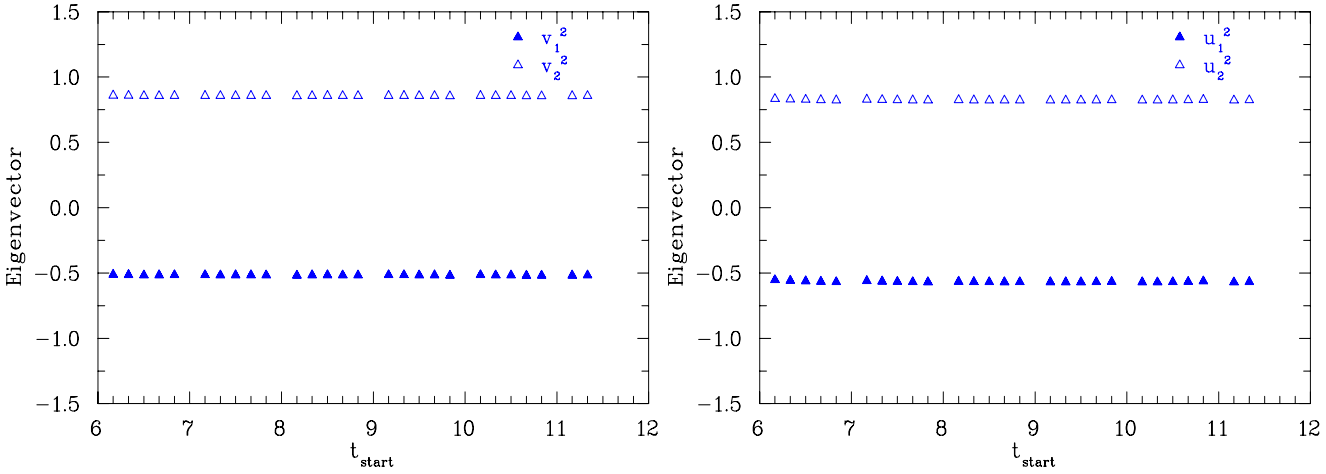

FIG. 8: (Color online). As in Fig. 7, but for the correlation matrix analysis of Fig. 6 and for the excited state.

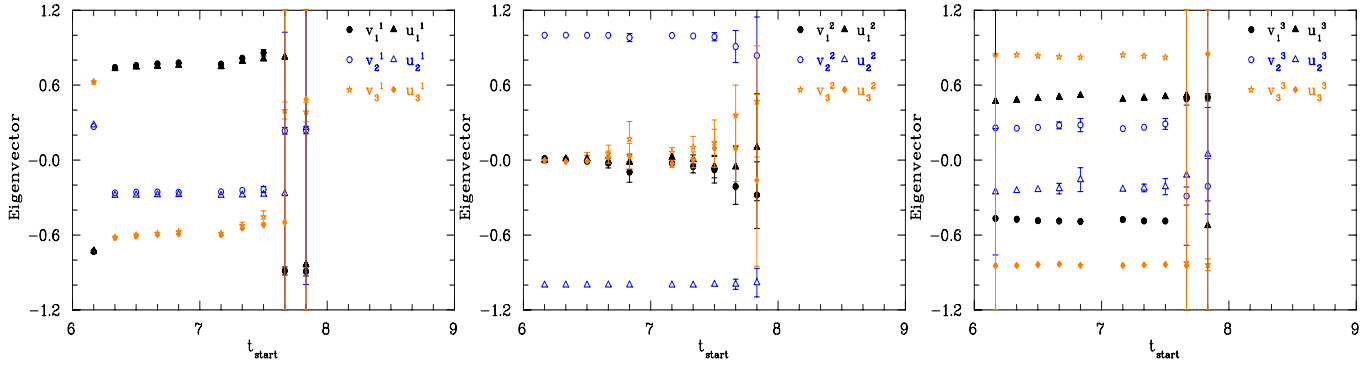

FIG. 9: (Color online). Eigenvector values of v_i^α and u_i^α, for the 3×3 correlation matrix analysis of χ_1, χ_2 and χ_4 interpolators, for **point source** to **point sink** correlation functions and for the pion mass of 797 MeV. The left figure corresponds to the contributions of the interpolators to the ground state, while middle and right figures are for the first and second excited states.

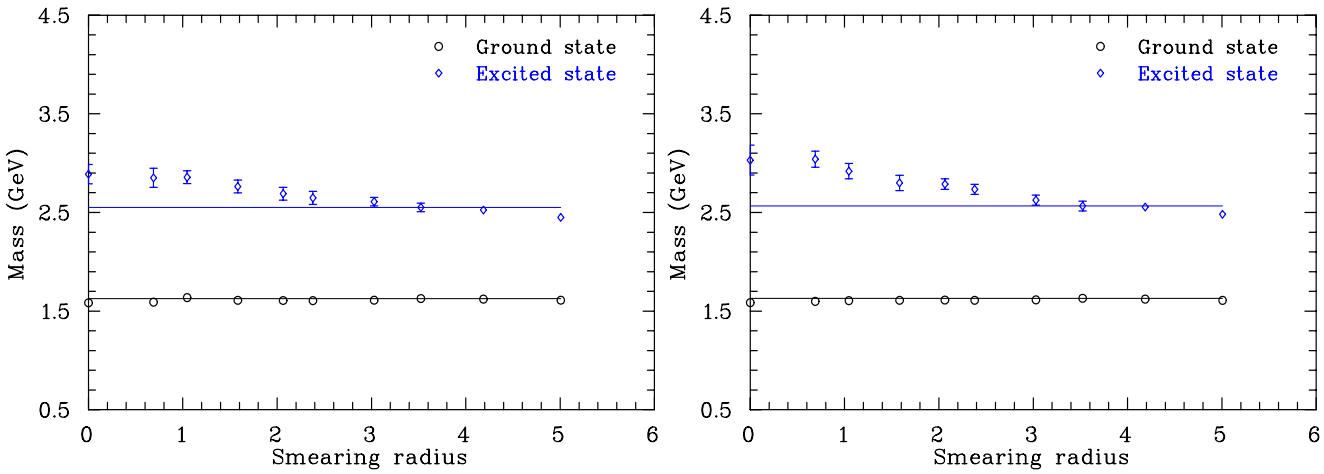

FIG. 10: (Color online). Mass of the nucleon ($N^{\frac{1}{2}^+}$) from the projected correlation functions for the pion mass of 797 MeV, for **point** (leftmost point) and for the **source smeared** to **point sink** correlation functions (all other points) with rms radii 0.6897, 1.0459, 1.5831, 2.0639, 2.3792, 3.0284, 3.5237, 4.1868, 5.0067, for 2×2 correlation matrices of χ_1, χ_2 (left) and χ_1, χ_4 (right). Horizontal lines are drawn through the points corresponding to radius 3.5237.

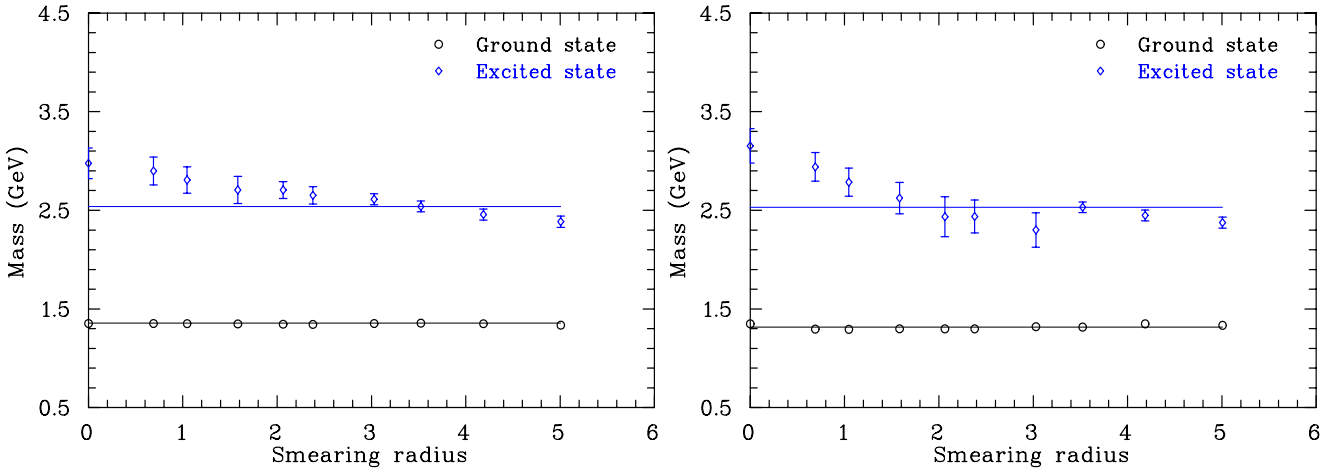

FIG. 11: (Color online). As in Fig. 10, but for the pion mass of 541 MeV (lightest).

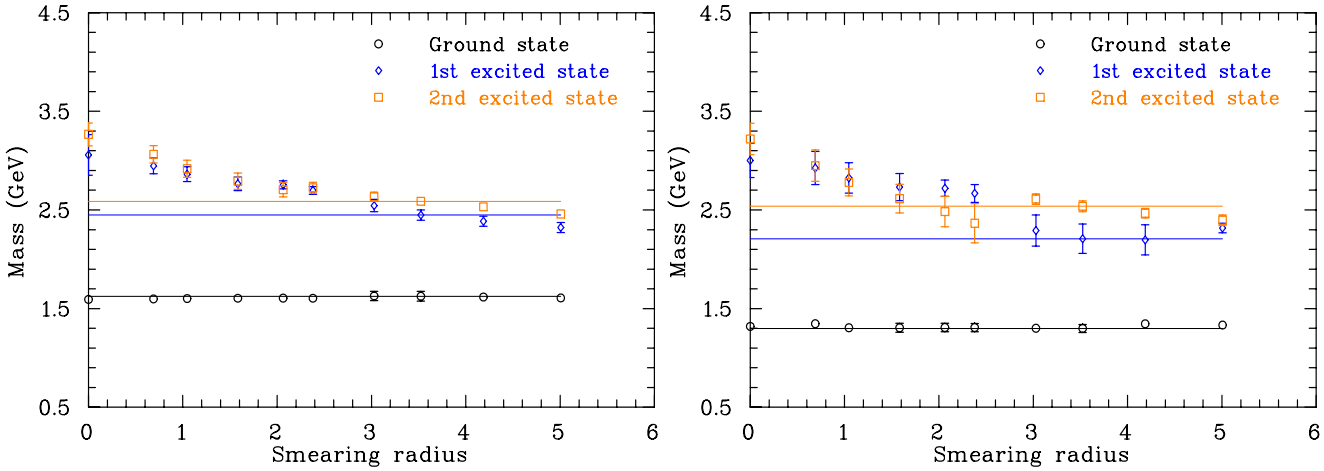

FIG. 12: (Color online). As in Fig. 10, but for the 3×3 correlation matrix of χ_1, χ_2 and χ_4 interpolators. The left figure corresponds to the pion mass of 797 MeV, whereas the right figure corresponds to a 541 MeV pion mass.

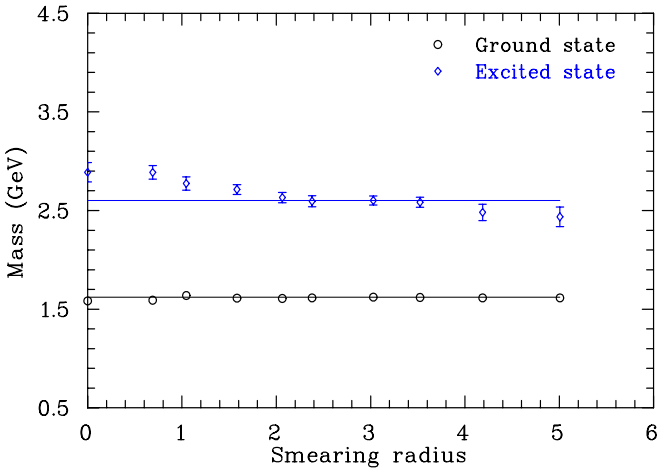

FIG. 13: (Color online). Mass of the nucleon ($N^{\frac{1}{2}^+}$) from the projected correlation functions for the pion mass of 797 MeV, for **point** (leftmost point) and for **smeared-smeared** correlation functions (all other points) with rms radii 0.6897, 1.0459, 1.5831, 2.0639, 2.3792, 3.0284, 3.5237, 4.1868, 5.0067, for 2×2 correlation matrices of χ_1,χ_2 interpolators. Straight lines are drawn through the points corresponding to radius 3.0284.

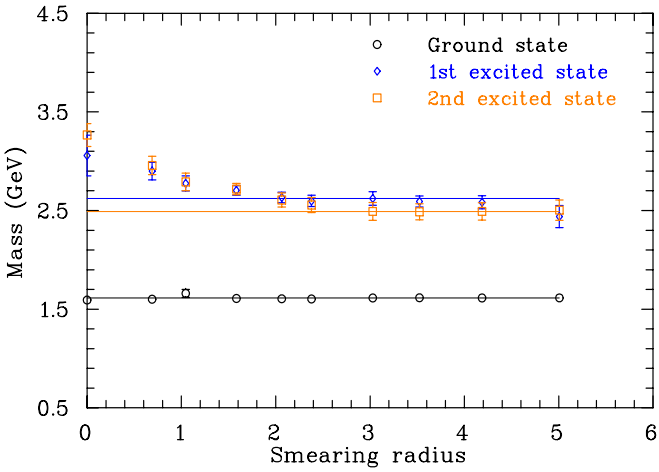

FIG. 14: (Color online). As in Fig. 13, but for the 3×3 correlation matrix of χ_1, χ_2 and χ_4 interpolators.

correlation function is analysed using standard analysis techniques.

To reduce human intervention in the fitting procedure, a fitting algorithm has been developed which is governed by specific fitting criteria based on the maximization of the fit window and the minimization of the value of the χ^2/dof while commencing at the earliest time-slice possible.

This study has shown for the first time that the excited state masses are fermion-source smearing dependent for all three types of smearing combinations; *i.e.*, the smeared source with point sink, the point source with smeared sink and smeared-smeared combinations. This is a somewhat unexpected result given that the ground state mass is independent of smearing.

All our 3×3 correlation matrix analyses provide two nearly degenerate excited-state masses. However, our concern is that these two masses correspond to strongly mixed QCD eigenstates that our analysis using the standard correlation matrix of χ_1, χ_2 and χ_4 interpolators is unable to resolve.

In particular, this technique has been used by several research collaborations to determine the mass of the Roper resonance [31, 43]. Remarkably, mass estimates based on these correlation matrix techniques tend to sit high relative to other approaches. This investigation provides a plausible explanation for these discrepancies.

Finally, it is clear that changing the smearing level of the

fermion source and sink changes the relative overlap of the superposition of the true eigenstates of QCD. Thus it would be interesting to use the robust analysis techniques presented here with large correlation matrices built not only on the χ_1, χ_2 and χ_4 interpolators but also on several levels of fermion-source and -sink smearing. This will be the subject of a future investigation.

Acknowledgments

We thank the NCI National Facility and eResearch SA for generous grants of supercomputing time which have enabled this project. This research is supported by the Australian Research Council.

[1] T. Burch et al., Phys. Rev. **D74**, 014504 (2006), hep-lat/0604019.
[2] N. Isgur and G. Karl, Phys. Lett. **B72**, 109 (1977).
[3] N. Isgur and G. Karl, Phys. Rev. **D19**, 2653 (1979).
[4] Z.-p. Li, V. Burkert, and Z.-j. Li, Phys. Rev. **D46**, 70 (1992).
[5] C. E. Carlson and N. C. Mukhopadhyay, Phys. Rev. Lett. **67**, 3745 (1991).
[6] P. A. M. Guichon, Phys. Lett. **B164**, 361 (1985).
[7] O. Krehl, C. Hanhart, S. Krewald, and J. Speth, Phys. Rev. **C62**, 025207 (2000), nucl-th/9911080.
[8] D. B. Leinweber, Phys. Rev. **D51**, 6383 (1995), nucl-th/9406001.
[9] F. X. Lee and D. B. Leinweber, Nucl. Phys. Proc. Suppl. **73**, 258 (1999), hep-lat/9809095.
[10] M. Gockeler et al. (QCDSF), Phys. Lett. **B532**, 63 (2002), hep-lat/0106022.
[11] S. Sasaki, T. Blum, and S. Ohta, Phys. Rev. **D65**, 074503 (2002), hep-lat/0102010.
[12] W. Melnitchouk et al., Phys. Rev. **D67**, 114506 (2003), hep-lat/0202022.
[13] R. G. Edwards, U. M. Heller, and D. G. Richards (LHP), Nucl. Phys. Proc. Suppl. **119**, 305 (2003), hep-lat/0303004.
[14] F. X. Lee et al., Nucl. Phys. Proc. Suppl. **119**, 296 (2003), hep-lat/0208070.
[15] N. Mathur et al., Phys. Lett. **B605**, 137 (2005), hep-ph/0306199.
[16] S. Sasaki, Prog. Theor. Phys. Suppl. **151**, 143 (2003), nucl-th/0305014.
[17] K. Sasaki, S. Sasaki, and T. Hatsuda, Phys. Lett. **B623**, 208 (2005), hep-lat/0504020.
[18] G. P. Lepage et al., Nucl. Phys. Proc. Suppl. **106**, 12 (2002), hep-lat/0110175.
[19] C. Morningstar, Nucl. Phys. Proc. Suppl. **109A**, 185 (2002), hep-lat/0112023.
[20] S. Sasaki, K. Sasaki, T. Hatsuda, and M. Asakawa, Nucl. Phys. Proc. Suppl. **119**, 302 (2003), hep-lat/0209059.
[21] K. Sasaki, S. Sasaki, T. Hatsuda, and M. Asakawa, Nucl. Phys. Proc. Suppl. **129**, 212 (2004), hep-lat/0309177.
[22] Y. Nakahara, M. Asakawa, and T. Hatsuda, Phys. Rev. **D60**, 091503 (1999), hep-lat/9905034.
[23] C. Allton, D. Blythe, and J. Clowser, Nucl. Phys. Proc. Suppl. **109A**, 192 (2002), hep-lat/0202024.
[24] M. Asakawa, T. Hatsuda, and Y. Nakahara, Prog. Part. Nucl. Phys. **46**, 459 (2001), hep-lat/0011040.
[25] C. Michael, Nucl. Phys. **B259**, 58 (1985).
[26] M. Luscher and U. Wolff, Nucl. Phys. **B339**, 222 (1990).
[27] C. McNeile and C. Michael (UKQCD), Phys. Rev. **D63**, 114503 (2001), hep-lat/0010019.
[28] C. R. Allton et al. (UKQCD), Phys. Rev. **D47**, 5128 (1993), hep-lat/9303009.
[29] J. M. Zanotti et al. (CSSM Lattice), Phys. Rev. **D68**, 054506 (2003), hep-lat/0304001.
[30] J. N. Hedditch, D. B. Leinweber, A. G. Williams, and J. M. Zanotti, Nucl. Phys. Proc. Suppl. **128**, 221 (2004), hep-lat/0402016.
[31] B. G. Lasscock et al., Phys. Rev. **D76**, 054510 (2007), 0705.0861.
[32] D. Brommel et al. (Bern-Graz-Regensburg), Phys. Rev. **D69**, 094513 (2004), hep-ph/0307073.
[33] T. Burch et al. (Bern-Graz-Regensburg), Phys. Rev. **D70**, 054502 (2004), hep-lat/0405006.
[34] T. Burch et al. (BGR(Bern-Graz-Regensburg)), Nucl. Phys. Proc. Suppl. **140**, 284 (2005), hep-lat/0409014.
[35] T. Burch et al., Nucl. Phys. **A755**, 481 (2005), nucl-th/0501025.
[36] B. G. Lasscock et al., Phys. Rev. **D72**, 014502 (2005), hep-lat/0503008.
[37] T. Burch, C. Gattringer, L. Y. Glozman, C. Hagen, and C. B. Lang, Phys. Rev. **D73**, 017502 (2006), hep-lat/0511054.
[38] T. Burch et al., Phys. Rev. **D73**, 094505 (2006), hep-lat/0601026.
[39] T. Burch et al., PoS **LAT2005**, 075 (2006), hep-lat/0509051.
[40] T. Burch et al., PoS **LAT2005**, 097 (2006), hep-lat/0509086.
[41] S. Basak et al., Nucl. Phys. Proc. Suppl. **153**, 242 (2006), hep-lat/0601034.
[42] S. Basak et al., Phys. Rev. **D76**, 074504 (2007), arXiv:0709.0008 [hep-lat].
[43] M. S. Mahbub et al., Phys. Lett. **B679**, 418 (2009), 0906.5433.
[44] S. Gusken, Nucl. Phys. Proc. Suppl. **17**, 361 (1990).
[45] B. G. Lasscock et al., Phys. Rev. **D72**, 074507 (2005), hep-lat/0504015.
[46] C. Alexandrou et al. (ETM), PoS **LAT2007**, 087 (2007), 0710.1173.
[47] C. Alexandrou et al. (European Twisted Mass), Phys. Rev. **D78**, 014509 (2008), 0803.3190.
[48] D. G. Richards et al. (LHPC), Nucl. Phys. Proc. Suppl. **109A**, 89 (2002), hep-lat/0112031.
[49] J. N. Hedditch, D. B. Leinweber, A. G. Williams, and J. M. Zanotti, Nucl. Phys. Proc. Suppl. **129**, 248 (2004), hep-lat/0309119.
[50] T. Takaishi, Phys. Rev. **D54**, 1050 (1996).
[51] P. de Forcrand et al. (QCD-TARO), Nucl. Phys. **B577**, 263 (2000), hep-lat/9911033.
[52] J. M. Zanotti et al. (CSSM Lattice), Phys. Rev. **D65**, 074507 (2002), hep-lat/0110216.
[53] J. M. Zanotti, B. Lasscock, D. B. Leinweber, and A. G. Williams, Phys. Rev. **D71**, 034510 (2005), hep-lat/0405015.

[54] R. Sommer, Nucl. Phys. **B411**, 839 (1994), hep-lat/9310022.
[55] C. Morningstar and M. J. Peardon, Phys. Rev. **D69**, 054501 (2004), hep-lat/0311018.
[56] D. B. Leinweber, R. M. Woloshyn, and T. Draper, Phys. Rev. **D43**, 1659 (1991).
[57] A. O. Cais, D. Leinweber, S. Mahbub, and T. Williams, PoS **LAT2008**, 137 (2008), 0812.1872.
[58] C. Alexandrou, C. N. Papanicolas, and E. Stiliaris (2008), 0810.3982.
[59] K. C. Bowler et al., Nucl. Phys. **B240**, 213 (1984).
[60] B. Blossier, G. von Hippel, T. Mendes, R. Sommer, and M. Della Morte, PoS **LATTICE2008**, 135 (2008), 0808.1017.
[61] B. Blossier, M. Della Morte, G. von Hippel, T. Mendes, and R. Sommer, JHEP **04**, 094 (2009), 0902.1265.